Supporting Information

Dynamic behavior of chemically tunable mechano-responsive hydrogels

Santidan Biswas, Victor V. Yashin, Anna C. Balazs*
Chemical Engineering Department, University of Pittsburgh, Pittsburgh, PA 15261, United States
* balazs@pitt.edu

S1. Reaction rate constants

The rate constants for the rupture and formation of labile bonds between the cryptic sites, k_r and k_f, respectively, are calculated as in our previous study.[1,2] When a subchain encompassing a closed loop is stretched, the force acting on the labile bond connecting the two cryptic sites increases and hence, facilitates bond rupture. We utilize the Bell model[3] to calculate the rupture rate constant as a function of the distance between the chain ends, R:

$$k_r(R) = k_r^{(0)} \exp[\gamma_R F_n(R) / k_B T] \tag{S1.1}$$

Here, $k_r^{(0)}$ is the rate of rupture at zero force, and $F_n(R)$ is the force applied to the ends of a polymer chain, which contains n Kuhn segments. Note that n is the number of segments in the part of the network subchain that does not form a loop. Finally, γ_R characterizes the sensitivity of the bond to the applied force; k_B and T are the respective Boltzmann's constant and temperature.

The force $F_n(R)$ is calculated according to the freely-jointed chain model (FJC): [4]

$$F_n(R) = \frac{k_B T}{b} \mathcal{L}^{-1}[R(nb)^{-1}] \quad , \tag{S1.2}$$

where

$$\mathcal{L}(x) = \coth(x) - x^{-1} \tag{S1.3}$$

is the Langevin function, and b is the length of the Kuhn segment. Through eq. (S1.2), we take into account the finite extensibility of a polymer chain. The force build up due to the finite extensibility has a strong effect on the bond rupture rate.

The rate constant for forming a labile bond between the cryptic sites, $k_f(R)$, depends on the chain end-to-end distance R. To form a bond, the reactive units in the unfolded chain of $n+l$ segments must first come into contact, and the probability of contact, P_c, depends on R. When in contact, the reactive units form a labile bond with the rate constant $k_f^{(0)}$, and hence $k_f(R) = P_c(R) k_f^{(0)}$. As in previous studies,[2,5–9] it is assumed that $k_f^{(0)}$ does not depend on the force acting on the bond. The probability of contact, $P_c(R)$, is calculated using the conformational statistics of the polymer chain: $P_c(R) = P_n(R) P_l(0) / P_{n+l}(R)$, where $P_n(R)$ is the probability distribution function for finding the ends of a chain of n segments at distance R apart. For the FJC model, this distribution function is [4]

$$P_n(R) = \frac{[\mathcal{L}^{-1}(x)]^2}{(2\pi n b^2)^{3/2} x \{1 - [\mathcal{L}^{-1}(x) \operatorname{csch}(\mathcal{L}^{-1}(x))]^2\}^{1/2}} \left[\frac{\sinh \mathcal{L}^{-1}(x)}{\mathcal{L}^{-1}(x)}\right]^n \exp[-nx\mathcal{L}^{-1}(x)] \tag{S1.4}$$

where $x = R(nb)^{-1}$. Note that through the equations for $P_c(R)$, the rate of chain folding depends on both the total length of the chain, $n+l$, and the length of the loop, l.

It is convenient to re-write the dimensionless variable $x = R(nb)^{-1}$ in eqs. (S1.3) and (S1.4) in terms of the chain extension λ. As mentioned above, we assume that all the loops are folded when the gel is in the undeformed state. Given that b is the length of one Kuhn segment, and there are l segments in one closed loop, the average end-to-end distance of an unperturbed chain is thus $R_0 = b\sqrt{n}$. The chain extension, λ, can be calculated as $R = \lambda R_0$, where R is the end-to-end distance of a deformed chain containing a closed loop and hence, $x = \lambda\, n^{-1/2}$ in eqs. (S1.3) and (S1.4). The rate constants of bond rupture and formation can now be expressed as functions of λ instead of R, i.e., $k_r(\lambda)$ and $k_f(\lambda)$, respectively.

The rate constant for complex formation in eq. (2) in the main text, K_{compl}, is proportional to the probability that the two reacting monomeric units will meet. We employ the scaling approach by Ito, *et al.*,[10] to account for the restrictions imposed by the polymer network on the binding of the dangling chains to the exposed cryptic sites. We obtain the following equation for the complexation rate constant as a function of the volume fraction of polymer ϕ:

$$K_{compl}(\phi) = K_0 \exp[-(a_0/b)^{4/3}(n+m+l)^{-1/3}\phi^{-2/3}] \qquad \text{(S1.5)}$$

The rate constant for the unbinding of a dangling chain in eq. (2), K_{uB}, is calculated similar to the rate constant of unfolding, eq. (S1.1), i.e., K_{uB} is a function of the chain extension λ

$$K_{uB}(\lambda) = k_{uB}^{(0)} \exp[\gamma_{uB} F_m(\lambda)/k_B T] \quad . \qquad \text{(S1.6)}$$

Here, $F_m(\lambda) = \dfrac{k_B T}{b}\mathcal{L}^{-1}[\lambda\, m^{-1/2}]$ is the force acting on a chain consisting of m segments under an extension λ (eq. (S1.2)), and $k_{uB}^{(0)}$ and γ_{uB} are the respective reaction rate constant at zero force and the force sensitivity parameter. Finally, K_0 is the rate constant of complex formation and a_0 is the size of a monomer.

S2. Free energy density of the gel system

The energy density of a deformed material, $u(I_1, I_3)$, can be specified as a function of the first I_1 and third I_3 invariants of the Finger strain tensor, $\hat{\mathbf{B}}$.

The total energy, $U_{tot} = v_0^{-1} k_B T \int u(I_1, I_3) dV_0$, is determined by integrating over the volume of the unstrained material, V_0. Here, $v_0 = a_0^3$ is the volume of a monomeric unit and the factor $v_0^{-1} k_B T$ is the unit of stress in our model.

In our model, there are three different contributions to the energy density:

1. $u_{\mathrm{el}}(I_1, I_3)$ describes the elastic energy of the permanently cross-linked network composed of FJC chains[2,11] within the approximation of affine deformations;
2. $u_{\mathrm{FH}}(I_3)$ describes the polymer-solvent interaction according to the Flory-Huggins model;

3. $u_{\mathrm{el}}^{*}(t)$ describes the contribution of the temporary cross-links to the elastic energy of the network.

The dimensionless energy density of the system is thus composed of:

$$u(I_1, I_3) = u_{\mathrm{el}}(I_1, I_3) + u_{\mathrm{FH}}(I_3) + u_{\mathrm{el}}^{*}(t) \tag{S2.1}$$

The first term on the right-hand side (r.h.s.) of eq. (11), $u_{\mathrm{el}}(I_1, I_3)$, is given by

$$\begin{aligned} u_{\mathrm{el}}(I_1, I_3) = {} & \frac{c_0 v_0}{2}\left[(1-p_U)\Psi(I_1, n) + p_U \Psi(I_1, n(1+l/n)^2) + \Psi(I_1, n+l)\right] \\ & - \frac{c_0 v_0}{4}\left[\zeta_0(n) + \zeta_0(n+l)\right] \ln I_3^{1/2} \end{aligned} \tag{S2.2}$$

Here, c_0 is the total concentration of subchains in the as-prepared gel.

The function $\Psi(I_1, n_{\mathrm{el}})$ is defined as

$$\Psi(I_1, n_{\mathrm{el}}) = n_{\mathrm{el}}\left[\psi\left(\sqrt{\frac{I_1}{3n_{\mathrm{el}}}}\right) - \psi(n_{\mathrm{el}}^{-1/2})\right] \tag{S2.3}$$

and gives the contribution to the elastic energy from a stretched FJC chain consisting of n_{el} elastically active segments. In eq. (S2.3), the function $\psi(x)$ in the antiderivative of the inverse Langevin function

$$\psi(x) = x\mathcal{L}^{-1}(x) + \ln\left(\frac{\mathcal{L}^{-1}(x)}{\sinh[\mathcal{L}^{-1}(x)]}\right) \quad .$$

The function $\zeta(x)$ is related to the inverse Langevin function and is defined as

$$\zeta(x) = (3x)^{-1}\mathcal{L}^{-1}(x) \quad .$$

Finally, $\zeta_0(n) = \zeta(n^{-1/2})$ as is mentioned in the main text after eq. (7).

We assume that all the subchains between cross-links have $n+l$ Kuhn segments, and the loops are folded in the un-deformed gel. Also, we assume that the amount of the subchains that contain loops is equal to the amount that contain dangling chains. The first term on the r.h.s. of eq. (S2.2) describes the entropic elasticity of the stretched polymer chains. There are three contributions to the total entropic elasticity:

1. fraction of subchains with folded loops for which $n_{\mathrm{el}} = n$;
2. fraction of subchains having unfolded loops for which $n_{\mathrm{el}} = n(1+l/n)^2$. The number of elastically active segments for the unfolded configuration is taken to be equal to the effective number $n_{\mathrm{el}} = n(1+l/n)^2$ because in the calculations of the rate of folding, the subchains with folded and unfolded loops are considered to have the same end-to-end distances.
3. contribution of the rest of the subchains that contain dangling chains for which $n_{\mathrm{el}} = n+l$.

The second term on the r.h.s of eq. (S2.2) accounts for the contribution of an ideal gas of permanent cross-link points. The second term on the r.h.s. of eq. (S2.1) is

$$u_{\mathrm{FH}}(I_3) = I_3^{1/2}\left[(1-\phi)\ln(1-\phi) + \chi_{FH}(\phi, T)\phi(1-\phi)\right] \tag{S2.4}$$

In eq. (S2.4), $\chi_{FH}(\phi,T)$ is the Flory-Huggins interaction parameter, and ϕ is the volume fraction of polymer. Note that ϕ depends on I_3 as $\phi=\phi_0 I_3^{-1/2}$, where ϕ_0 is the volume fraction of polymer in the un-deformed state, and

The dangling chains contribute to the elastic energy only when they form temporary cross-links by attaching to the exposed cryptic bonds. The last term on the r.h.s. of eq. (S2.1) describes the contribution to the energy density from the temporary cross-links:

$$u_{\mathrm{el}}^{*}(t)=c_0^{*}v_0\xi(t,0)\left[\Psi(I_1(t,0),m)-\frac{\zeta_0(m)}{2}\ln(I_3^{1/2}(t,0))\right] + c_0^{*}v_0\int_0^t\frac{\partial\xi}{\partial\tau}(t,\tau)\left[\Psi(I_1(t,\tau),m)-\frac{\zeta_0(m)}{2}\ln(I_3^{1/2}(t,\tau))\right]d\tau \quad \text{(S2.5)}$$

Equation (S2.5) is a generalization of eq. (S2.2) to the case of transient networks. Here, deformations at a given time are affected by deformations that occurred earlier in the sample.[12,13] Specifically, the stress tensor within a transient network depends on the relative strain tensor $\hat{\mathbf{b}}(t,\tau)$, which characterizes deformations in the network at time *t* relative to the (deformed) state of the network at τ. Correspondingly, $u_{\mathrm{el}}^{*}(t)$ depends on the invariants of the relative strain tensor $I_1(t,\tau)$ and $I_3(t,\tau)$.[13] It is worth noting that $\hat{\mathbf{b}}(t,0)=\hat{\mathbf{B}}(t)$.

As described in the main text, the function $\xi(t,\tau)$ on the r.h.s. of eq. (S2.5) determines the number of cross-links that were created before the time τ and still exist at time $t\geq\tau$. The time derivative $\partial\xi(t,\tau)/\partial\tau$ determines the number of cross-links that exist at time t and were created during the period of time from τ to $\tau+d\tau$. The detailed expressions of $\xi(t,\tau)$ and $\partial\xi(t,\tau)/\partial\tau$ are provided in the main text (Eqs. 5 and 6).

S3. Computational model (gLSM)

The 3D gel lattice spring model (gLSM) computational technique[1,14–16] allows us to simulate the dynamic behavior of the gels along with the kinetics of unfolding and binding of loops and dangling chains with reactive ends. The gLSM is a finite element approximation, and utilizes the combination of finite element and finite difference approaches to numerically solve the elastodynamic equations characterizing the behavior of chemo-responsive polymer gels. The gLSM has been utilized in modeling thermo-responsive gels, and have yielded good agreements with corresponding experimental results. For instance, the gLSM was initially developed to simulate the dynamic behavior of self-oscillating polymer gels undergoing the Belousov-Zhabotinsky (BZ) reaction [14–18] and to predict the response of these BZ gels to an applied force.[19–22]

The gLSM was further modified to include chromophores that undergo a light-induced isomerization reaction,[23–25] and used for simulations of the dynamics of such photo-responsive gels. Additionally, we modeled and provided optimization guidelines of the self-regulating behavior of chemically-reactive microposts embedded in a thermo-responsive gel.[26] Recently, we augmented our 3D gLSM to take into account the finite extensibility of the chains within gels containing loops.[1] In this paper, we utilize the model that accounted for the dynamic (temporary) binding of dangling chains.[2]

The gLSM is based on the two-fluid, polymer and solvent, model for polymer networks.[27–29] The dynamics of the polymer network is assumed to be purely relaxational, so that the forces acting on the swollen, deformed gel are balanced by the frictional drag due to the motion of the solvent. It is also assumed that the polymer-solvent inter-diffusion is the sole contribution to the gel dynamics. Hence, the velocity of the polymer, $\mathbf{v}^{(p)}$, can be calculated as [15]

$$\mathbf{v}^{(p)} = \Lambda_0(\phi/\phi_0)^{-3/2}(1-\phi)\nabla\cdot\hat{\boldsymbol{\sigma}} \tag{S3.1}$$

where Λ_0 is the kinetic coefficient, which is inversely proportional to the polymer-solvent friction coefficient η_0. In the simulations, we choose some l_0 and t_0 for the respective units of length and time, and stress is measured in the units of $\sigma_0 = k_BT/v_0$, where v_0 is the volume of a monomeric unit within a polymer chain. The dimensionless kinetic coefficient Λ_0 is calculated as $\Lambda_0 = k_BT(v_0\eta_0 l_0^2 t_0^{-1})^{-1}$.[15]

Within the gLSM framework, a 3D gel sample is represented by a set of linear hexahedral elements[30,31] and consists of $(L_x-1)\times(L_y-1)\times(L_z-1)$ identical cubic elements. Here, L_i is the number of nodes in the i-direction, $i = x, y, z$. Initially, the sample is undeformed and each element is characterized by the same volume fraction ϕ_0 and cross-link density c_0. (Note that the cross-link density is equal to the concentration of elastically active subchains in the network.) Upon deformation, the elements move together with the polymer network so that the amount of polymer and number of permanent cross-links within each hexahedral element remain equal to their initial values. Correspondingly, the volume fraction of polymer in the element $\mathbf{m} \equiv (i, j, k)$ is determined as $\phi(\mathbf{m}) = \phi_0\Delta^3/V(\mathbf{m})$, where Δ and $V(\mathbf{m})$ are the undeformed element size and volume of the deformed element, respectively.

The gel dynamics is described through the motion of the nodes of the elements caused by forces acting on these nodes. For the gel model considered here, the energy density is dimensionless and is composed of three terms:

$$u(I_1, I_3) = u_{\mathrm{el}}(I_1, I_3) + u_{\mathrm{FH}}(I_3) + u^*_{\mathrm{el}}(t) \tag{S3.2}$$

Here, the first term on the right-hand side (r.h.s.) of eq. (S3.2), $u_{\mathrm{el}}(I_1, I_3)$, describes the elastic energy of the crosslinked network, $u_{\mathrm{FH}}(I_3)$ describes the polymer-solvent interaction according to the Flory-Huggins model, and $u^*_{\mathrm{el}}(t)$ is the elastic energy contribution from the temporary cross-links.

We use the finite element approximation (FEA) to determine the element energy density $u(\mathbf{m})$ from $u(I_1, I_3)$ in eq. (S3.2).[16] The total energy of the gel is then

$$U_{tot} = \Delta^3 \sum\nolimits_{\mathbf{m}} u(\mathbf{m}) \tag{S3.3}$$

where the contribution from the element $\mathbf{m}$, $u(\mathbf{m})$, depends only on the coordinates of the nodes of this element denoted as $\boldsymbol{x}_n(\mathbf{m})$, $n = 1, 2, ..., 8$. (Note that $u(\mathbf{m})$ is the gel energy per unit volume of the undeformed element.) Then, the force acting on each node is given by the equation

$$\mathbf{F}_n(\mathbf{m}) = -\frac{\partial U_{tot}}{\partial \boldsymbol{x}_n(\mathbf{m})} \tag{S3.4}$$

The right hand side of the above equation contains contributions from all elements adjacent to a given node (in order to consider all the elements belonging to a common node). Finally, we consider over-damped dynamics and thus the velocity of the node is proportional to the force and is given by

$$\frac{d\boldsymbol{x}_n(\mathbf{m})}{dt} = M_n(\mathbf{m})\mathbf{F}_n(\mathbf{m}) \tag{S3.5}$$

where $M_n(\mathbf{m})$ is the mobility of the node proportional to the kinetic coefficient Λ_0 mentioned above.

The contributions to $u(\mathbf{m})$ and $\mathbf{F}_n(\mathbf{m})$ due to the elastic energy of permanent network and the polymer solvent interactions, i.e., the first three terms on the r.h.s. of eq. (S3.2), and the mobility $M_n(\mathbf{m})$ are calculated as described in detail in ref.[2] Below, we focus solely on applying the FEA to the last term on the r.h.s. of eq. (S3.2), $u^*_{\mathrm{el}}(t)$, that then gives the contribution of the temporary cross-links to the nodal forces.

Equation for $u^*_{\mathrm{el}}(t)$ is given as follows:

$$\begin{aligned} u^*_{el}(t) &= -\frac{c_0 v_0}{2}\zeta_0(m)p_B(t)\ln I_3^{1/2}(t) \\ &+\frac{c_0 v_0}{2}\xi(t,0)\zeta(\lambda(t)m^{-1/2})I_1(t)+\frac{c_0 v_0}{2}\int_0^t \frac{\partial \xi}{\partial \tau}(t,\tau)\zeta(\lambda(t,\tau)m^{-1/2})I_1(t,\tau)d\tau \end{aligned} \tag{S3.6}$$

where we omit the terms, which do not contribute to the stress-strain relationship, eq. (10) in the main text. It is seen that the first and second terms on the r.h.s. of eq. (S3.6) depend on the first, $I_1(t)$, and third, $I_3(t)$, invariants of the Finger strain tensor $\hat{\mathbf{B}}(t)$. Therefore, application of the FEA to the latter two terms is the same as described in ref.[16] Hence, the main step in the gLSM formulation of $u^*_{\mathrm{el}}(t)$ is the FEA of the last term on the r.h.s. of eq. (S3.6) that depends on the invariant $I_1(t,\tau)$ of the relative Finger strain tensor $\hat{\mathbf{b}}(t,\tau)$. We start with the following decomposition of the relative strain tensor:

$$\hat{\mathbf{b}}(t,\tau) = \hat{\mathbf{F}}(t)\cdot\hat{\mathbf{C}}^{-1}(\tau)\cdot\hat{\mathbf{F}}^{\mathrm{T}}(t) \tag{S3.7}$$

Here, $\hat{\mathbf{F}}(t)$ is the deformation-gradient tensor associated with the deformation $\boldsymbol{X}\to\boldsymbol{x}(\boldsymbol{X},t)$

$$[\hat{\mathbf{F}}(t)]_{ij} = \frac{dx_i(\boldsymbol{X},t)}{dX_j}, \quad i,j=1,2,3$$

and $\hat{\mathbf{C}}(t)$ is the left Cauchy-Green strain tensor (the Cauchy-Green strain tensor)

$$\hat{\mathbf{C}}(t) = \hat{\mathbf{F}}^{\mathrm{T}}(t)\cdot\hat{\mathbf{F}}(t) \tag{S3.8}$$

The superscript "T" stands for the transposition operation. The first relative strain invariant is defined as $I_1(t,\tau) = \mathrm{tr}\,\hat{\mathbf{b}}(t,\tau)$, so it can be equivalently written in the following way

$$I_1(t,\tau)) = \mathrm{tr}[\hat{\mathbf{C}}^{-1}(\tau)\cdot\hat{\mathbf{C}}(t)] \tag{S3.9}$$

The components of the Cauchy-Green strain tensor can be calculated as

$$[\hat{\mathbf{C}}(t)]_{ij} = \mathbf{g}_i(t)\cdot\mathbf{g}_j(t) \tag{S3.10}$$

where $\mathbf{g}_i(t)$ are the base vectors

$$\mathbf{g}_i(t) = \frac{\partial \boldsymbol{x}(\boldsymbol{X},t)}{\partial X_i}, \quad i = 1,2,3 \tag{S3.11}$$

The matrix elements of $\hat{\mathbf{C}}^{-1}$ can be calculated analytically as

$$[\hat{\mathbf{C}}^{-1}]_{ij} = \varepsilon_{ikl}\varepsilon_{jmn}\frac{(\mathbf{g}_k \times \mathbf{g}_l)\cdot(\mathbf{g}_m \times \mathbf{g}_n)}{(\mathbf{g}_1 \cdot (\mathbf{g}_2 \times \mathbf{g}_3))^2} \tag{S3.12}$$

In the above equation, ε_{ijk} is the Levi-Civita symbol, so the sets of indexes (i,k,l) and (j,m,n) are the cyclic permutations of $(1,2,3)$. No summation over the repeated indexes is performed in eq. (S3.12).

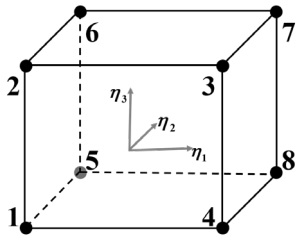

Fig. S1 Schematic of the 3D hexahedral element. The local coordinate system $\boldsymbol{\eta} = (\eta_1, \eta_2, \eta_3)$ is placed in the center of element. The labels $1,2,\ldots,8$ indicate the local node numbering within the element.

Within each linear hexahedral element, the three functions, which specify the deformation $\boldsymbol{x}(\boldsymbol{X},t)$, are approximated by a tri-linear expansion. Then, the reference local coordinate system $\boldsymbol{\eta} = (\eta_1, \eta_2, \eta_3)$, where $-1 \le \eta_i \le 1$, $i = 1,2,3$, is introduced within each element (see Fig. S1).[30,31] The coordinates within the element $\mathbf{m}$ in this reference coordinate system can be calculated through the values of the nodal coordinates, $\boldsymbol{x}_n(\mathbf{m},t)$, and a set of "shape functions" $N_n(\boldsymbol{\eta}) \equiv N_n(\eta_1,\eta_2,\eta_3)$, $1 \le n \le 8$, as explained in ref.[16]

$$\boldsymbol{x}(t) = \sum_{n=1}^{8} \boldsymbol{x}_n(\mathbf{m},t) N_n(\boldsymbol{\eta}) \tag{S3.13}$$

Within the above finite element approximation, the base vectors, eq. (S3.11), are calculated as

$$\mathbf{g}_i(\mathbf{m},t) = 2\Delta^{-1}\sum_{n=1}^{8} \boldsymbol{x}_n(\mathbf{m},t)\frac{\partial N_n}{\partial \eta_i} \tag{S3.14}$$

Substituting eq. (S3.14) into eqs. (S3.9),(S3.10) and (S3.12) yields the following equation for the relative strain invariant $I_1(t,\tau)$ in the element $\mathbf{m}$

$$I_1(t,\tau) = \Delta^{-2}\sum_{n,m=1}^{8} \Gamma_{nm}(\mathbf{m},\tau)(\boldsymbol{x}_n(\mathbf{m},t)\cdot\boldsymbol{x}_m(\mathbf{m},t)) \tag{S3.15}$$

The above equation exhibits two important features, namely, the pairwise contribution of the nodes, and factorization of the t- and τ-dependences in each term. The τ-dependent matrix elements $\Gamma_{nm}(\tau)$ in the quadratic form, eq. (S3.15), are determined according to eq. (S3.9) as

$$\Gamma_{nm}(\tau) = 4 \sum_{i,j=1}^{3} [\hat{\mathbf{C}}^{-1}(\tau)]_{ij} \frac{\partial N_n}{\partial \eta_j} \frac{\partial N_m}{\partial \eta_i} \tag{S3.16}$$

In the above equation, we omitted the dependence of Γ_{nm} on the element number $\mathbf{m}$ for the sake of simplicity. Further, the matrix elements $\Gamma_{nm}(\tau)$ exhibit the following properties:

$$\Gamma_{nm} = \Gamma_{mn}, \sum_{n=1}^{8} \Gamma_{nm} = 0 \tag{S3.17}$$

Within each element $\mathbf{m}$, the values $\Gamma_{nm}(\mathbf{m}, \tau)$ depend on the nodal coordinates at the moment of time τ, $\boldsymbol{x}_n(\mathbf{m}, \tau)$, and on the reference element coordinates $\boldsymbol{\eta}$.

Substituting eqs. (S3.15) and (S3.16) into the last term on the r.h.s. of eq. (S3.6) and integrating it over the volume of undeformed element $\mathbf{m}$ gives the following result denoted as $u^*(\mathbf{m}, t)$:

$$u^*(\mathbf{m}, t) = \Delta^{-2} \frac{c_0 v_0}{2} \sum_{n,k=1}^{8} \theta_{nk}(\mathbf{m}, t)(\boldsymbol{x}_n(\mathbf{m}, t) \cdot \boldsymbol{x}_k(\mathbf{m}, t)) \quad , \tag{S3.18}$$

where

$$\theta_{nk}(\mathbf{m}, t) = \int_0^t \frac{\partial \xi}{\partial \tau}(t, \tau) \zeta(\lambda(t, \tau) m^{-1/2}) \rho_{nk}(\mathbf{m}, \tau) d\tau \quad , \tag{S3.19}$$

and $\partial \xi(t, \tau) / \partial \tau$ is defined by eq. (6).The values $\rho_{nk}(\mathbf{m}, \tau)$ on the r.h.s. of eq. (S3.19) are obtained by integration of the matrix elements $\Gamma_{nm}(t)$ defined by eq. (S3.16) over the reference element volume:

$$\rho_{nm}(\mathbf{m}, t) = \frac{1}{8} \int \Gamma_{nm}(\mathbf{m}, \boldsymbol{\eta}, t) d\boldsymbol{\xi} \tag{S3.20}$$

Note that the above equation explicitly shows the dependence of Γ_{nm} on the reference element coordinates $\boldsymbol{\eta}$. The contribution of eq. (S3.17) to the force acting on the node *n* of the element $\mathbf{m}$ from other nodes within the same element is

$$\mathbf{F}_n^*(\mathbf{m}, t) \equiv -\Delta^3 \frac{\partial u^*(\mathbf{m}, t)}{\partial \boldsymbol{x}_n(\mathbf{m}, t)} = c_0 v_0 \Delta \sum_{k \neq n} \theta_{nk}(\mathbf{m}, t)(\boldsymbol{x}_n(\mathbf{m}, t) - \boldsymbol{x}_k(\mathbf{m}, t)) \tag{S3.21}$$

where we utilized the properties of the Γ_{nm} given by eq. (S3.17). Equation (S3.21) shows that within the gLSM approach, the contribution of the temporary cross-links to the nodal forces is described by a system of linear springs with the time-dependent spring stiffness $\theta_{nk}(\mathbf{m}, t)$.

Equation (S3.21) is a formal solution of the problem because evaluating $\theta_{nk}(\mathbf{m}, t)$ requires further simplifications. First of all, the integration in eq. (S3.20) cannot be performed analytically. The integral can be calculated approximately through the Gaussian quadrature. We use the simplest Gaussian quadrature, which corresponds to approximating the integrand function by its value at the element center, $\boldsymbol{\eta} = (0, 0, 0) \equiv \mathbf{0}$, to obtain

$$\rho_{nk}(\mathbf{m}, \tau) \approx \Gamma_{nk}(\mathbf{m}, \mathbf{0}, \tau) \tag{S3.22}$$

Under the above approximation, the matrix elements ρ_{nk} exhibit the following symmetry properties additional to that in eq. (S3.17):

$$\rho_{n1} = -\rho_{n7},\ \rho_{n2} = -\rho_{n8},\ \rho_{n3} = -\rho_{n5},\ \rho_{n4} = -\rho_{n6}$$

at any $1 \le n \le 8$. Since the matrix elements θ_{nk} exhibit the same symmetry properties as ρ_{nk}, the nodal force $\mathbf{F}_n^*(\mathbf{m},t)$ under the approximation in eq. (S3.22) can be conveniently written in the following form:

$$\mathbf{F}_n^*(\mathbf{m},t) = c_0 v_0 \Delta \sum_{k=1}^{4} \theta_{nk}(\mathbf{m},t)\,\mathbf{d}_k(\mathbf{m},t), \quad 1 \le n \le 8, \tag{S3.23}$$

where $\mathbf{d}_k$, $1 \le k \le 4$, are the vectors defining the main diagonals of the element:

$$\mathbf{d}_1 = \boldsymbol{x}_7 - \boldsymbol{x}_1,\ \mathbf{d}_2 = \boldsymbol{x}_8 - \boldsymbol{x}_2,\ \mathbf{d}_3 = \boldsymbol{x}_5 - \boldsymbol{x}_3,\ \mathbf{d}_4 = \boldsymbol{x}_6 - \boldsymbol{x}_4 \tag{S3.24}$$

Evaluating the matrix $[\hat{\mathbf{C}}^{-1}]_{ij}$, eq. (S3.12), is also simplified because at $\boldsymbol{\eta} = \mathbf{0}$, the base vectors, eq. (S3.11), are calculated through the main diagonals, eq. (S3.24), as

$$\mathbf{g}_1 = (4\Delta)^{-1}(\mathbf{d}_1 + \mathbf{d}_2 - \mathbf{d}_3 - \mathbf{d}_4) \quad ,$$

$$\mathbf{g}_2 = (4\Delta)^{-1}(\mathbf{d}_1 + \mathbf{d}_2 + \mathbf{d}_3 + \mathbf{d}_4) \quad ,$$

$$\mathbf{g}_3 = (4\Delta)^{-1}(\mathbf{d}_1 - \mathbf{d}_2 - \mathbf{d}_3 + \mathbf{d}_4) \quad .$$

In addition, using the approximation in eq. (S3.22) reduces the number of linearly independent values of θ_{nk} in the equation for the force, eq. (S3.23), down to 6.

Finally, evaluation of the spring stiffness matrix elements $\theta_{nk}(\mathbf{m},t)$, eq. (S3.19), is performed through the numerical integration over τ, and $\partial\xi(t,\tau)/\partial\tau$ is given by eq. (6) in the main text. For this purpose, the 3-point Simpson's integration rule is used. Note this integration requires the values of the deformation history from $\tau \to -\infty$ to time t. Numerically, the numerical integration might become computationally expensive, so that the array size is limited to certain value. We choose the array size to assure that the stored history of deformation is enough to attain convergence to the steady state limits. In our calculations, the array size of 5000 was found sufficient for convergence to the steady state values. At every current time step, we applied a first-in last-out array replacement to remove the past deformation and move in the present time deformation history into the stored arrays.

We focus on the state of equilibrium swelling of a gel that contains both cryptic bonds and dangling chains with reactive ends. To calculate the equilibrium shear and Young's elastic moduli, we utilize the basic definitions of these moduli. Namely, each modulus is calculated as a corresponding stress to strain ratio in the limit of small deformations. The dimensionless kinetic coefficient is $\Lambda_0 = 100$.[16] In our gLSM simulations, the dimensionless units of time and length correspond to ~1s and ~ 40 μm, respectively, for the given choice of parameters. We carried out the gLSM simulations using a single element sample. The time step used for the gLSM simulations is $\Delta t = 0.001$. Figure 3 in the main text presents the results of the gLSM simulations.

In order to obtain the storage and loss dynamic moduli, we performed the gLSM simulations of a sinusoidal shear deformation of a single element. In Fig. S2, we plot the dynamic shear modulus as a function of dimensionless frequency, $\omega / K_{uB}^{(st)}$, at $T = 15°\text{C}$. The points represent the values of the dynamic modulus obtained from the gLSM simulation. The lines

represent the values of dynamic shear modulus obtained from the linearized theory (see eq. S4.14). The shear deformation is volume preserving. The exact match between the two results corroborate that for small deformation, the linearized approximation yields proper result.

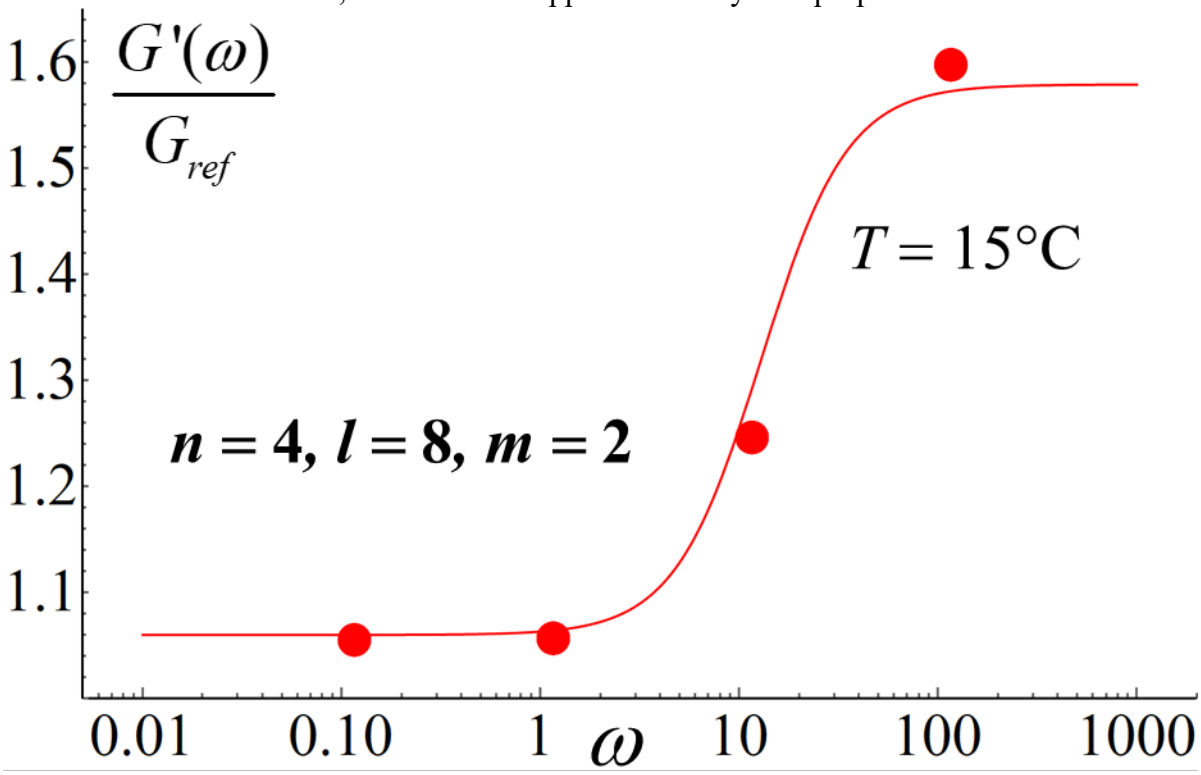

Fig. S2 The dynamic storage shear modulus G' as a function of dimensionless frequency $\omega / K_{uB}^{(st)}$ at $T = 15°\text{C}$ for the System IV normalized with the value of G_{ref}. The solid line shows the values calculated using eq. (S4.14). The solid disks represent the modulus values obtained through the gLSM simulations.

S4. Calculations of elastic moduli

The stress tensor $\hat{\boldsymbol{\sigma}}$ for the gel system with loops and dangling chains with reactive ends is given in main text in eqs. (7)-(10). The steady state of the gel is obtained when $\hat{\boldsymbol{\sigma}} = 0$.

Without relaxation, linearization of the stress tensor results in

$$\delta\hat{\boldsymbol{\sigma}}(t) = \lambda\,\mathrm{tr}[\hat{\boldsymbol{\varepsilon}}(t)]\hat{\mathbf{I}} + 2\mu\,\hat{\boldsymbol{\varepsilon}}(t) \tag{S4.1}$$

where λ and μ are the first and second Lame parameters, respectively, and $\hat{\mathbf{I}}$ is the unit tensor. The shear G and bulk K moduli are related to the Lame parameters as

$$G = \mu \tag{S4.2}$$

$$K = \lambda + \frac{2}{3}\mu \tag{S4.3}$$

Young's modulus E is calculated as

$$E = \frac{9KG}{3K + G} \tag{S4.4}$$

If relaxation takes place, the Lame parameters become the convolution kernels, and the stress-strain equation is conveniently formulated via the Fourier transform:

$$\delta\hat{\boldsymbol{\sigma}}_\omega = \lambda_\omega \,\mathrm{tr}(\hat{\boldsymbol{\varepsilon}}_\omega)\,\hat{\mathbf{I}} + 2\mu_\omega\,\hat{\boldsymbol{\varepsilon}}_\omega \tag{S4.5}$$

The Fourier transform is defined here as $f_\omega = \int_{-\infty}^{+\infty} f(t)\exp(-i\omega t)dt$. The shear G_ω and bulk K_ω moduli are related to the Lame parameters as

$$G_\omega = \mu_\omega \tag{S4.6}$$

$$K_\omega = \lambda_\omega + \frac{2}{3}\mu_\omega \tag{S4.7}$$

Young's modulus E_ω is calculated as

$$E_\omega = \frac{9K_\omega G_\omega}{3K_\omega + G_\omega} \tag{S4.8}$$

Dynamic shear moduli

After linearization, the contributions to the stress tensor $\delta\hat{\boldsymbol{\sigma}}^{(sh)}(t)$ that are linear in strain $\hat{\boldsymbol{\varepsilon}}$ are

$$\begin{aligned}\delta\hat{\boldsymbol{\sigma}}^{(sh)}(t) = {} & \frac{c_0}{2\lambda_{st}}\left[(1-p_U^{(st)})\,\zeta\left(\frac{\lambda_{st}}{\sqrt{n}}\right) + p_U^{(st)}\,\zeta\left(\frac{\lambda_{st}\sqrt{n}}{n+l}\right) + \zeta\left(\frac{\lambda_{st}}{\sqrt{n+l}}\right)\right]\times 2\,\hat{\boldsymbol{\varepsilon}}(t) \\ & + 2c_0\zeta_0(m)\frac{\phi_{st}}{\phi_0}\,p_B^{(st)}\left[\hat{\boldsymbol{\varepsilon}}(t) - K_{uB}^{(st)}\int_{-\infty}^{t} \mathrm{e}^{-K_{uB}^{(st)}(t-\tau)}\,\hat{\boldsymbol{\varepsilon}}(\tau)d\tau\right]\end{aligned} \tag{S4.9}$$

The equilibrium shear modulus G_0 comparing equations S4.9 with S4.1 yields

$$G_0 = \frac{c_0}{2\lambda_{st}}\left[(1-p_U^{(st)})\,\zeta\left(\frac{\lambda_{st}}{\sqrt{n}}\right) + p_U^{(st)}\,\zeta\left(\frac{\lambda_{st}\sqrt{n}}{n+l}\right) + \zeta\left(\frac{\lambda_{st}}{\sqrt{n+l}}\right)\right] \tag{S4.10}$$

When relaxation is considered, the fourier transform of the above equation S4.9 yields

$$\delta\hat{\boldsymbol{\sigma}}_\omega^{(sh)} = \left(G_0 + \Delta G\frac{i\omega / K_{uB}^{(st)}}{1 + i\omega / K_{uB}^{(st)}}\right)\times 2\,\hat{\boldsymbol{\varepsilon}}_\omega \tag{S4.11}$$

and hence, the complex dynamic dynamic shear modulus G_ω is

$$G_\omega = G_0 + \Delta G\frac{i\omega / K_{uB}^{(st)}}{1 + i\omega / K_{uB}^{(st)}} \tag{S4.12}$$

Here,

$$\Delta G = c_0\zeta_0(m)\frac{\phi_{st}}{\phi_0}\,p_B^{(st)} \tag{S4.13}$$

The storage and loss shear moduli are:

$$G'(\omega) = G_0 + \Delta G\frac{(\omega / K_{uB}^{(st)})^2}{1 + (\omega / K_{uB}^{(st)})^2} \tag{S4.14}$$

$$G''(\omega) = \Delta G \frac{\omega / K_{uB}^{(st)}}{1 + (\omega / K_{uB}^{(st)})^2} \tag{S4.15}$$

Using the values obtained from solving the gel systems at equilibrium into the shear modulus formula, we obtain the values of the modulus numerically for both the equilibrium scenario as well as for the frequency dependent values.

Dynamic bulk moduli

The spatially isotropic contributions to the stress tensor due to variations of volume are expressed as:

$$\begin{aligned} \delta\hat{\boldsymbol{\sigma}}^{(v)}(t) = & \left[-\phi_{st} \left(\frac{\partial \sigma_{vol}}{\partial \phi} \right)_{st} + \frac{\lambda_{st}}{3} \left(\frac{\partial \sigma_{vol}}{\partial \bar{\lambda}} \right)_{st} \right] \mathrm{tr}[\hat{\boldsymbol{\varepsilon}}(t)] \hat{\mathbf{I}} \\ & + \left[\left(\frac{\partial \sigma_{vol}}{\partial p_U} \right)_{st} \delta p_U(t) + \left(\frac{\partial \sigma_{vol}}{\partial p_B} \right)_{st} \delta p_B(t) \right] \hat{\mathbf{I}} \end{aligned} \tag{S4.16}$$

Here,

$$\begin{aligned} \sigma_{vol} = & \frac{c_0 \lambda_{st}^2}{2} \frac{\phi}{\phi_0} \left[(1 - p_U) \zeta \left(\frac{\bar{\lambda}}{\sqrt{n}} \right) + p_U \zeta \left(\frac{\bar{\lambda}\sqrt{n}}{n+l} \right) + \zeta \left(\frac{\bar{\lambda}}{\sqrt{n+l}} \right) \right] \\ & + c_0 \zeta_0(m) p_B \frac{\phi}{2\phi_0} - \left(\pi_{FH}(\phi) + c_0 [\zeta_0(n) + \zeta_0(n+l)] \frac{\phi}{4\phi_0} \right) \end{aligned} \tag{S4.17}$$

The partial derivatives of σ_{vol} are calculated as follows:

$$-\phi_{st} \left(\frac{\partial \sigma_{vol}}{\partial \phi} \right)_{st} = \left(\phi \frac{\partial \pi_{FH}}{\partial \phi} - \pi_{FH} \right)_{st}$$

$$\frac{\lambda_{st}}{3} \left(\frac{\partial \sigma_{vol}}{\partial \bar{\lambda}} \right)_{st} = \frac{c_0}{6\sqrt{n}} \left[(1 - p_U^{(st)}) \zeta' \left(\frac{\lambda_{st}}{\sqrt{n}} \right) + p_U^{(st)} \frac{n}{n+l} \zeta' \left(\frac{\lambda_{st}\sqrt{n}}{n+l} \right) + \sqrt{\frac{n}{n+l}} \zeta' \left(\frac{\lambda_{st}}{\sqrt{n+l}} \right) \right]$$

$$\left(\frac{\partial \sigma_{vol}}{\partial p_U} \right)_{st} = \frac{c_0}{2\lambda_{st}} \left[\zeta \left(\frac{\lambda_{st}\sqrt{n}}{n+l} \right) - \zeta \left(\frac{\lambda_{st}}{\sqrt{n}} \right) \right]$$

$$\left(\frac{\partial \sigma_{vol}}{\partial p_B} \right)_{st} = c_0 \zeta_0(m) \frac{\phi_{st}}{2\phi_0}$$

Note that $-\phi_{st} \left(\partial \sigma_{vol} / \partial \phi \right)_{st}$ is the osmotic compressibility.

The volumetric stress is affected by unfolding and binding through the terms proportional to $\delta p_U(t)$ and $\delta p_B(t)$, respectively, which, in turn, are linear functionals of $\mathrm{tr}\,\hat{\boldsymbol{\varepsilon}}(t)$.

Linearization of the non-linear chemical kinetics equations for p_U and p_B

$$dp_U/dt = k_r (1 - p_U) - k_f (1 - \pi_B)^2 p_U$$

$$dp_B/dt = \phi_0^{-1} \phi c_0 K_{compl} p_U (1 - \pi_B)(1 - p_B) - K_{uB} p_B$$

results in the following linear equations for δp_U and δp_B

$$\frac{d}{dt}\begin{pmatrix}\delta p_U\\ \delta p_B\end{pmatrix}+\begin{pmatrix}\Gamma_{UU} & \Gamma_{UB}\\ \Gamma_{BU} & \Gamma_{BB}\end{pmatrix}\begin{pmatrix}\delta p_U\\ \delta p_B\end{pmatrix}=\begin{pmatrix}\delta K_U\\ \delta K_B\end{pmatrix}\mathrm{tr}\,\hat{\boldsymbol{\varepsilon}}(t)$$

Here,

$$\Gamma_{UU}=k_r^{(st)}\frac{p_U(1-p_B)+p_B(1-p_U)}{p_U(p_U-p_B)}$$

$$\Gamma_{UB}=-2k_r^{(st)}\frac{1-p_U}{p_U-p_B}$$

$$\Gamma_{BU}=-K_{uB}^{(st)}\frac{p_B}{p_U-p_B}$$

$$\Gamma_{BB}=K_{uB}^{(st)}\frac{p_U-p_B^2}{(1-p_B)(p_U-p_B)}$$

$$\delta K_U=k_r^{(st)}(1-p_U)\frac{\lambda_{st}}{3}\left(\frac{\partial}{\partial\bar{\lambda}}\log\frac{k_r}{k_f}\right)_{st}$$

$$\delta K_B=-K_{uB}^{(st)}p_B\left[\phi_{st}\left(\frac{\partial}{\partial\phi}\log K_c\right)_{st}+\frac{\bar{\lambda}}{3}\left(\frac{\partial}{\partial\bar{\lambda}}\log K_{uB}\right)_{st}\right]$$

For simplicity, the subscript "(st)" is omitted in $p_U^{(st)}$ and $p_B^{(st)}$ in the above equations. The equilibrium bulk modulus K is obtained comparing equations S4.16 with S4.1 and S4.3.

For the dynamic moduli, the equations for δp_U and δp_B are solved in terms of the Fourier transforms:

$$\begin{pmatrix}\delta p_{U\omega}\\ \delta p_{B\omega}\end{pmatrix}=(i\omega\hat{\mathbf{I}}+\hat{\boldsymbol{\Gamma}})^{-1}\begin{pmatrix}\delta K_U\\ \delta K_B\end{pmatrix}\mathrm{tr}\,\hat{\boldsymbol{\varepsilon}}_\omega$$

Finally, the complex dynamic bulk modulus K_ω is obtained in the following form:

$$K_\omega=\left(\phi^2\frac{\partial}{\partial\phi}\left(\frac{\pi_{FH}}{\phi}\right)+\frac{\bar{\lambda}}{3}\frac{\partial\sigma_{vol}}{\partial\bar{\lambda}}\right)_{st}+\begin{pmatrix}\left(\frac{\partial\sigma_{vol}}{\partial p_U}\right)_{st} & \left(\frac{\partial\sigma_{vol}}{\partial p_B}\right)_{st}\end{pmatrix}(i\omega\hat{\mathbf{I}}+\hat{\boldsymbol{\Gamma}})^{-1}\begin{pmatrix}\delta K_U\\ \delta K_B\end{pmatrix}+\frac{2}{3}G_\omega \quad \text{(S4.18)}$$

S5. Finite shear and tensile deformations

The stress tensor $\hat{\boldsymbol{\sigma}}$ for the gel system with loops and dangling chains with reactive ends is given in main text in Eqs. 7-10. Below, we derive equations describing the shear and tensile deformations of gel in the general case of finite deformations. The elastic moduli could be obtained using the derived equations if the deformations are small.

Simple shear deformations

We consider a 3D cubic gel swollen to their equilibrium degree of swelling λ_{eq}. A simple shear is defined by the evolution of the node positions of the gel sample as follows:

$$x(t) = \lambda_{eq} X + \lambda_{eq} k(t) Y$$

$$y(t) = \lambda_{eq} Y$$

$$z(t) = \lambda_{eq} Z$$

Here, $k(t)$ is the time-dependent deformation. In the case of oscillatory shear, $k(t) = k_0 \sin(\omega t)$. Knowing the time-dependent coordinates, the Finger strain tensor, $\hat{\mathbf{B}}(t)$, and the relative Finger strain tensor, $\hat{\mathbf{b}}(t,\tau)$, are calculated as

$$\hat{\mathbf{B}}(t) = \lambda_{eq}^2 \begin{pmatrix} 1+k^2(t) & k(t) & 0 \\ k(t) & 1 & 0 \\ 0 & 0 & 1 \end{pmatrix}$$

$$\hat{\mathbf{b}}(t,\tau) = \begin{pmatrix} 1+[k(t)-k(\tau)]^2 & k(t)-k(\tau) & 0 \\ k(t)-k(\tau) & 1 & 0 \\ 0 & 0 & 1 \end{pmatrix}$$

The average strain, $\bar{\lambda}(t) \equiv \sqrt{I_1(t)/3}$, is calculated from the above equations as $\bar{\lambda}(t) = \lambda_{eq}\sqrt{1+k^2(t)/3}$. Similarly, the average relative strain is $\bar{\lambda}(t,\tau) = \sqrt{1+[k(t)-k(\tau)]^2/3}$. Thus, the shear stress $\sigma_{12}(t)$ at a given value of $k(t)$ can be calculated directly:

$$\sigma_{12}(t) = \frac{c_0}{2\lambda_{eq}}\left[(1-p_U(t))\zeta\left(\frac{\bar{\lambda}(t)}{\sqrt{n}}\right) + p_U(t)\zeta\left(\frac{\bar{\lambda}(t)\sqrt{n}}{n+l}\right) + \zeta\left(\frac{\bar{\lambda}(t)}{\sqrt{n+l}}\right)\right]k(t) + \frac{c_0^*}{\lambda_{eq}^3}\int_{-\infty}^{t}\frac{\partial\xi}{\partial\tau}(t,\tau)\zeta\left(\frac{\bar{\lambda}(t,\tau)}{\sqrt{m}}\right)[k(t)-k(\tau)]\,d\tau \quad \text{(S5.1)}$$

The time-dependent values $p_U(t)$ and $\frac{\partial\xi}{\partial\tau}(t,\tau)$ are calculated as described in the main text. Note eq. (S5.1) depends on the history of deformation. To numerically calculate the stress value, an integration over history of deformation needs to be performed.

Tensile deformations

We consider a 3D cubic gel swollen to their equilibrium degree of swelling λ_{eq}. Under a tensile deformation, the gel exhibits the degrees of swelling λ and λ_{tr} in the direction of deformation and normal to it, respectively. The Finger tensor and the relative tensor for this scenario is given by

$$\hat{\mathbf{B}}(t)=\begin{pmatrix}\lambda^2(t) & 0 & 0\\ 0 & \lambda_{tr}^2(t) & 0\\ 0 & 0 & \lambda_{tr}^2(t)\end{pmatrix}$$

$$\hat{\mathbf{b}}(t,\tau)=\begin{pmatrix}(\lambda(t)/\lambda(\tau))^2 & 0 & 0\\ 0 & (\lambda_{tr}(t)/\lambda_{tr}(\tau))^2 & 0\\ 0 & 0 & (\lambda_{tr}(t)/\lambda_{tr}(\tau))^2\end{pmatrix}$$

Note that the amount of polymer in gel does not change with deformation, so $\phi=\phi_0(\lambda\lambda_{tr}^2)^{-1}$.

The average strain, $\bar{\lambda}(t)$, and the average relative strain, $\bar{\lambda}(t,\tau)$, are calculated through the first invariants of the corresponding tensors to obtain

$$\bar{\lambda}(t)=3^{-1/2}\sqrt{\lambda^2(t)+2\lambda_{tr}^2(t)}$$

$$\bar{\lambda}(t,\tau)=3^{-1/2}\sqrt{(\lambda(t)/\lambda(\tau))^2+2(\lambda_{tr}(t)/\lambda_{tr}(\tau))^2}\,.$$

The stress component in the direction of deformation, i.e., the tensile stress, is calculated as:

$$\sigma(t)=c_0\Gamma(p_U(t),\bar{\lambda}(t))\frac{\phi(t)}{\phi_0}\lambda^2(t)-P(\phi(t),p_B(t))$$
$$+c_0^*\frac{\phi(t)}{\phi_0}\int_{-\infty}^{t}\frac{\partial\xi}{\partial\tau}(t,\tau)\zeta\left(\frac{\bar{\lambda}(t,\tau)}{\sqrt{m}}\right)\frac{\lambda^2(t)}{\lambda^2(\tau)}d\tau \qquad \text{(S5.2)}$$

The value of stress in the transverse direction is zero and therefore,

$$c_0\Gamma(p_U(t),\bar{\lambda}(t))\frac{\phi(t)}{\phi_0}\lambda_{tr}^2(t)-P(\phi(t),p_B(t))$$
$$+c_0^*\frac{\phi(t)}{\phi_0}\int_{-\infty}^{t}\frac{\partial\xi}{\partial\tau}(t,\tau)\zeta\left(\frac{\bar{\lambda}(t,\tau)}{\sqrt{m}}\right)\frac{\lambda_{tr}^2(t)}{\lambda_{tr}^2(\tau)}d\tau=0 \qquad \text{(S5.3)}$$

At a given tensile strain $\lambda(t)$, $\lambda_{tr}(t)$ is determined through solving eq. (S5.3). The time-dependent probabilities of unfolding, $p_U(t)$ and binding, $p_B(t)$, are calculated as described in the main text. Finally, eq. (S5.2) is used to calculate the tensile stress $\sigma(t)$.

S6. Effect of varying the rate constants

In our prior study,[1] we discussed the effects of the various parameters on the behavior of the gel system. For example, we determined the effect of the rate constants for bond rupture, k_r and formation, k_f, and the force sensitivity parameter, γ_R, on the probability of unfolding a loop, p_U. We further discussed how variations in p_U affect the steady-state chain extension λ for various values of γ_R. We demonstrated that the unfolding occurs at progressively lower chain extensions as the dimensionless parameter γ_R/b is increased. The latter parameter characterizes the sensitivity of bond rupture to force. (In ref. 1, the parameter γ_R was denoted γ_0.)

Furthermore, we showed that the degree of swelling increases as the number of Kuhn segments in the loop are increased.

In the latter study, [1] the system did not contain dangling chains with reactive ends. We now consider the possible interactions that involve the latter reactive ends and exposed, unfolded loop sites. In a subsequent paper, [2], we noted that all the parameters were chosen to highlight the difference between the case where the unfolded loops can bind to the reactive ends and the case where the ends of the dangling chains are non-reactive. We use the same parameters from the latter paper [2] in this work. We also assume that chain segments formed between unfolded loop sites and the dangling reactive ends cannot cross each other. In the calculations, we assume that the loops and dangling chains are relatively short. Specifically, we take 8 Kuhn segments for the loops, and 2 Kuhn segments for the dangling chains.

In the main text, we considered the case where $k_f^{(0)} / k_r^{(0)} = 2 \times 10^2$ and $k_C^{(0)} / k_{uB}^{(0)} = 2 \times 10^4$, i.e., $k_f^{(0)} / k_r^{(0)} < k_C^{(0)} / k_{uB}^{(0)}$. The text details how the configuration of four different systems depends on these rate constants and subsequently, how the configurations affect the degree of swelling. The detailed discussion of the latter findings can be found in the discussion of Fig. 3. The behavior for the dynamic moduli of the four systems was also discussed in the main text. This discussion can be found in the descriptions of Figs. 4 and 5.

Here, we show the effect of varying the rate constant of folding relative to that of bond rupture at zero force. To show the effect of the rate constants on the four systems, we keep the relative rate of complexation (at zero force) equal to $k_C^{(0)} / k_{uB}^{(0)} = 2 \times 10^4$, and increase the relative rate of folding $k_f^{(0)} / k_r^{(0)}$. Specifically, we consider the following two cases:

1) $k_f^{(0)} / k_r^{(0)} = 2 \times 10^4$ i.e., $k_f^{(0)} / k_r^{(0)} = k_C^{(0)} / k_{uB}^{(0)}$ (see Fig. S3).

2) $k_f^{(0)} / k_r^{(0)} = 2 \times 10^5$ i.e., $k_f^{(0)} / k_r^{(0)} > k_C^{(0)} / k_{uB}^{(0)}$ (see Fig. S4).

To facilitate the following discussion, we again define the four systems here. In System I (black), the loops are permanently in the unfolded state ($p_U = 1$ and $p_B = 0$), and the ends of the dangling chains are inert. System II (blue) is similar to System I (black), except that the loops can undergo a folding and unfolding transition, but the ends of the dangling chains remain inert. In System III, the dangling ends are again inert ($p_B = 0$), but the loops are permanently folded. In System IV, the loops can undergo reversible folding and unfolding, and the dangling linkers with reactive ends can bind to the exposed loop sites.

For case 1, $k_f^{(0)} / k_r^{(0)} = k_C^{(0)} / k_{uB}^{(0)} = 2 \times 10^4$ and thus, the rate constant of folding is much larger than the rate of unfolding. As noted above, in System II (blue), the loops can undergo a folding and unfolding transition, but the ends of the dangling chains remain inert. Still, for the high value of the rate constant of folding, most of the loops will remain folded even though unfolding is permitted. The blue curve for System II shows essentially the same degree of swelling as that for System III (green) where the loops are permanently folded.

Since most of the loops remain folded and $k_f^{(0)} / k_r^{(0)} = k_C^{(0)} / k_{uB}^{(0)}$, the fraction of reactive ends bound to exposed loops also decreases. The degree of swelling in gel System IV (red) becomes nearly equal to that the of System II (unfolding and no binding) except near the LCST

temperature. Near the transition temperature, some fraction of the unfolded chains are bound by the reactive ends of the linkers, and thus the degree of swelling exhibits a slight decrease (red curve) compared to the green and blue curves. The permanently unfolded and no binding units (black) show the most swelling since the loops are always open (Fig. S3(a)).

The loops in System I are always in the unfolded state and the ends of the dangling chains are not reactive and hence, the system does not form the temporary crosslinks that would stiffen the gel. Consequently, among the four systems, System I swells the most and offers the least resistance to deformation; this behavior is reflected in the lowest value of the equilibrium moduli (black) for both shear and tensile deformation.

Unlike System I, the other three systems behave like the system with permanently folded loops. The blue, green, and red curves for the equilibrium moduli effectively overlap (Figs. S3(b) and S3(c)) with each other, showing that such a high rate constant of folding diminishes the effect of the unfolding-folding transition. Additionally, both System II (blue) and IV (red) behave like System III, i.e., as if the loops are in permanently folded conformations. Figures S3(b) and S3(c) show that near the transition temperature, the moduli (red) has a higher value compared to the blue and green curves because some fraction of the unfolded chains are bound by the reactive ends of the linkers.

For case 2: $k_f^{(0)} / k_r^{(0)} > k_C^{(0)} / k_{uB}^{(0)}$, the blue, green, red curves effectively overlap with each other showing that at such high values, the rate constant of folding dominates the kinetics; unfolding and binding are greatly hindered from occurring. In effect, this parameter choice reduces System II (blue) and IV (red) to System III with permanently folded loops (green) (Fig. S4(a)-(c)).

The dynamic moduli (Fig. S3(d) –(f) and S4(d) – (f)) of the four systems also exhibit the behavior discussed in the main text. Only System IV (red) shows frequency-dependent behavior. Note, however, that since the self-stiffening was lower for this choice of rate constant, the value of the dynamic moduli for the system with binding (red curve) at higher frequency shows a lower increase compared to the dynamic moduli curves in the main text. For System I-III (respective black, blue and green curves), the dynamic moduli have a constant value equal to the equilibrium moduli. However, the choice of a higher rate constant of folding causes the system with unfolding but inert reactive ends (blue) to behave similarly to the System III (system with permanently folded loops). As a result, the green and the blue curves, (Fig. S3(d) –(f) and S4(d)-(f)), essentially overlap while in Fig. 4-5 in the main text, System II (blue) behaved more like System I (black) i.e., as if the loops were permanently unfolded.

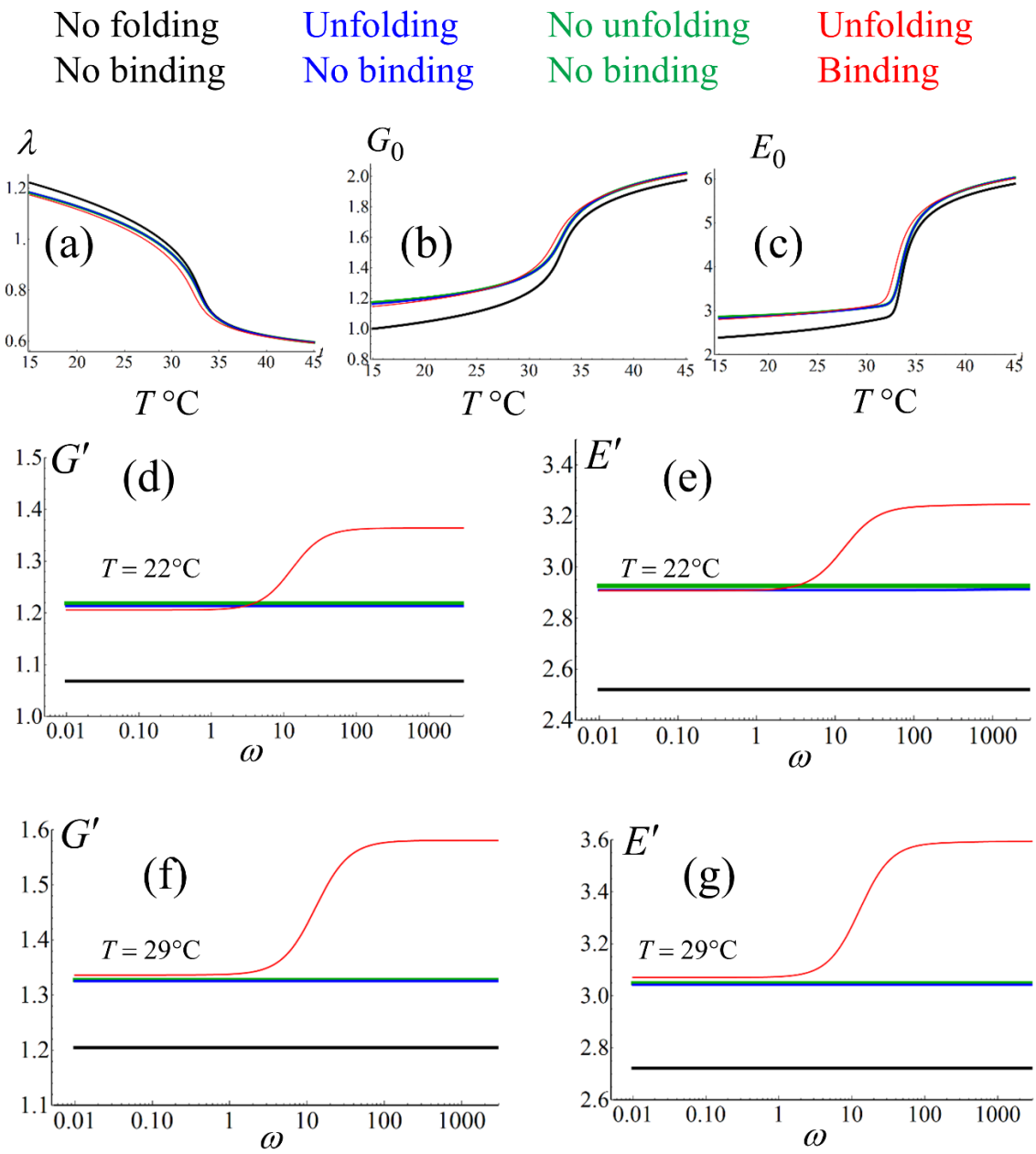

Figure S3. The equilibrium (a) lateral extensions λ, (b) shear moduli G_0, and (c) Young's moduli E_0 for the gel systems I – IV as functions of temperature. Panels (d) and (f) show the storage shear moduli G' as functions of the dimensionless frequency ω at $T = 22°C$ and $T = 29°C$, respectively. Panels (e) and (g) show the storage Young's moduli E' as functions of the dimensionless frequency $\omega / K_{uB}^{(st)}$ at $T = 22°C$ and $T = 29°C$, respectively. All moduli are scaled with respect to G_{ref}, which is the equilibrium shear modulus of the gel system I at $15°C$. The lines show the numerical solution obtained using *Mathematica*™. Calculations were performed at $k_f^{(0)} / k_r^{(0)} = k_C^{(0)} / k_{uB}^{(0)} = 2 \times 10^4$ and $k_C^{(0)} / k_{uB}^{(0)} = 2 \times 10^4$. All other model parameters are specified in text.

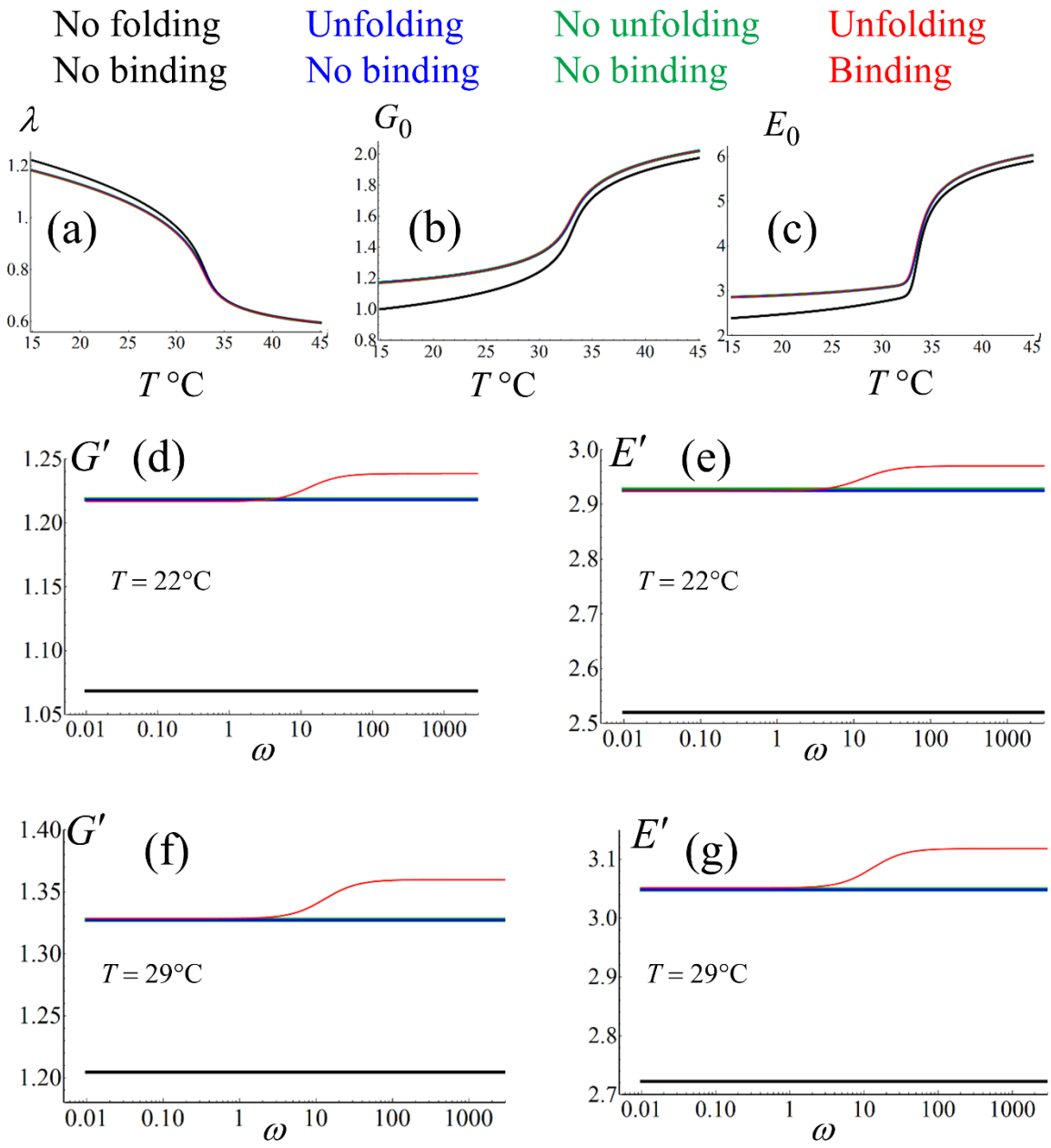

Figure S4. The same as in Fig. S3 obtained at $k_f^{(0)} / k_r^{(0)} = 2 \times 10^5$.

References

1 S. Biswas, V. V. Yashin and A. C. Balazs, *Soft Matter*, 2018, **14**, 3361–3371.

2 S. Biswas, V. V. Yashin and A. C. Balazs, *Soft Matter*, 2020, **16**, 5120–5131.

3 G. I. Bell, *Science*, 1978, **200**, 618–627.

4 M. Rubinstein and R. H. Colby, *Polymer Physics*, Oxford University Press, Oxford, 2003.

5 B. V. S. Iyer, V. V. Yashin, T. Kowalewski, K. Matyjaszewski and A. C. Balazs, *Polym. Chem.*, 2013, **4**, 4927–4939.

6 B. V. S. Iyer, I. G. Salib, V. V. Yashin, T. Kowalewski, K. Matyjaszewski and A. C.

Balazs, *Soft Matter*, 2013, **9**, 109–121.
7 M. J. Hamer, B. V. S. Iyer, V. V. Yashin and A. C. Balazs, *Nano Lett.*, 2014, **14**, 4745–4750.
8 M. J. Hamer, B. V. S. Iyer, V. V. Yashin, T. Kowalewski, K. Matyjaszewski and A. C. Balazs, *Soft Matter*, 2014, **10**, 1374–1383.
9 B. V. S. Iyer, V. V. Yashin, M. J. Hamer, T. Kowalewski, K. Matyjaszewski and A. C. Balazs, *Prog. Polym. Sci.*, 2015, **40**, 121–137.
10 K. Ito, J. Chuang, C. Alvarez-Lorenzo, T. Watanabe, N. Ando and A. Y. Grosberg, *Prog. Polym. Sci.*, 2003, **28**, 1489–1515.
11 L. Anand, *Comput. Mech.*, 1996, **18**, 339–355.
12 P. J. Flory, *Trans. Faraday Soc.*, 1960, **56**, 722–743.
13 A. D. Drozdov, *Finite Elasticity and Viscoelasticity*, World Scientific, Singapore, 1996.
14 V. V. Yashin and A. C. Balazs, *Science*, 2006, **314**, 798–801.
15 V. V. Yashin and A. C. Balazs, *J. Chem. Phys.*, 2007, **126**, 124707.
16 O. Kuksenok, V. V. Yashin and A. C. Balazs, *Phys. Rev. E - Stat. Nonlinear, Soft Matter Phys.*, 2008, **78**, 041406.
17 V. V. Yashin, O. Kuksenok and A. C. Balazs, *Prog. Polym. Sci.*, 2010, **35**, 155–173.
18 V. V. Yashin, O. Kuksenok, P. Dayal and A. C. Balazs, *Reports Prog. Phys.*, 2012, **75**, 066601.
19 O. Kuksenok, V. V. Yashin and A. C. Balazs, *Soft Matter*, 2009, **5**, 1835–1839.
20 V. V. Yashin, K. J. Van Vliet and A. C. Balazs, *Phys. Rev. E*, 2009, **79**, 046214.
21 V. V. Yashin, O. Kuksenok and A. C. Balazs, *J. Phys. Chem. B*, 2010, **114**, 6316–22.
22 I. C. Chen, O. Kuksenok, V. V. Yashin, A. C. Balazs and K. J. Van Vliet, *Adv. Funct. Mater.*, 2012, **22**, 2535–2541.
23 O. Kuksenok and A. C. Balazs, *Adv. Funct. Mater.*, 2013, **23**, 4601–4610.
24 O. Kuksenok and A. C. Balazs, *Sci. Rep.*, 2015, **5**, 9569.
25 O. Kuksenok and A. C. Balazs, *Mater. Horiz.*, 2016, **3**, 53–62.
26 X. He, M. Aizenberg, O. Kuksenok, L. D. Zarzar, A. Shastri, A. C. Balazs and J. Aizenberg, *Nature*, 2012, **487**, 214–218.
27 B. Barrière and L. Leibler, *J. Polym. Sci. Part B Polym. Phys.*, 2003, **41**, 166–182.
28 A. Onuki, *Adv. Polym. Sci.*, 1993, **109**, 63–121.
29 M. Doi, *J. Phys. Soc. Japan*, 2009, **78**, 052001.
30 I. M. Smith, D. V. Griffiths and L. Margetts, *Programming the Finite Element Method*, John Wiley & Sons, 2013.
31 O. C. Zienkiewicz, R. L. Taylor and J. Z. Zhu, *The Finite Element Method: Its Basis and Fundamentals*, Butterworth-Heinemann, 7th edn., 2013.